Sculpting of an erodible body by flowing water

Leif Ristroph[a,1], Matthew N. J. Moore[a], Stephen Childress[a], Michael J. Shelley[a], and Jun Zhang[a,b]

[a]Applied Mathematics Laboratory, Courant Institute, New York University, New York, NY 10012; and [b]Department of Physics, New York University, New York, NY 10003

Erosion by flowing fluids carves striking landforms on Earth and also provides important clues to the past and present environments of other worlds. In these processes, solid boundaries both influence and are shaped by the surrounding fluid, but the emergence of morphology as a result of this interaction is not well understood. We study the coevolution of shape and flow in the context of erodible bodies molded from clay and immersed in a fast, unidirectional water flow. Although commonly viewed as a smoothing process, we find that erosion sculpts pointed and cornerlike features that persist as the solid shrinks. We explain these observations using flow visualization and a fluid mechanical model in which the surface shear stress dictates the rate of material removal. Experiments and simulations show that this interaction ultimately leads to self-similarly receding boundaries and a unique front surface characterized by nearly uniform shear stress. This tendency toward conformity of stress offers a principle for understanding erosion in more complex geometries and flows, such as those present in nature.

geomorphology | fluid-structure interaction | abrasion | ablation | mechanical wear

Reflecting on his scientific discoveries, Isaac Newton compared himself to a boy on the seashore who marvels at having found a yet smoother stone (1). For pebbles and mountains alike, our curiosity about natural sculptures stems perhaps from the realization that these shapes reflect countless incremental events acting over eons. Morphology is often the only clue available as we attempt to reconstruct the physical history of the Earth as well as of our neighboring worlds (2–6). Recreating geologically inspired situations in the laboratory offers an opportunity to connect the development of structures to the underlying processes at work (7). This approach has been used to study phenomena across many scales, for example, the rounding of rocks by abrasion (8), the formation of rivers (9) and drainage channels (10), and the drift of continental plates driven by mantle convection (11).

Rather than mimic a particular geological scenario, we conduct experiments that isolate a central aspect common to all erosive processes: the interdependent evolution of shape and flow (3). As described in *Methods*, we study the erosion of soft clay bodies by fast-flowing water, allowing us to witness what is an intractably slow process in nature. We consider unidirectional flow and canonical initial geometries—a thin flat bed of clay, a cylinder, and a sphere—with an eye toward informing mathematical models that intimately link the coevolving flow and shape (12, 13). Our experiments typically involve centimeter-scale bodies immersed in flows of 40–70 cm/s, yielding high Reynolds numbers of order 10^4. Importantly, the solid boundaries recede at rates (approximately centimeters per hour) that are many orders slower than the flow speed, preserving the large separation of time-scales characteristic of natural erosion.

Considering first the case of a 3D body, we form a clay sphere of diameter 4.9 cm and support it within a water tunnel with a cross-section of 15×15 cm. After 70 min in the 46-cm/s flow, erosion has sculpted surprisingly sharp features, as shown by the photograph of the body in Fig. 1A. A nearly conical nose has formed on the upstream surface, whereas further downstream two distinct ridges encircle the body, followed by a flattened back. The emergence and persistence of these points, corners, and facets seem to defy the conventional wisdom that erosion yields rounded and smooth surfaces.

To determine how these peculiar geometrical features relate to the surrounding flow, we seed the fluid with particles and illuminate a plane near the midsection of the body. The photograph in Fig. 1B reveals the streaklines 10 min into the erosion process, and an interpretation of this flow structure is given in Fig. 1D. The incoming stream meets the sharpening nose at the stagnation point, and the flow conforms to the surface until separating at a slight ridge on the body. Downstream of this separation line, vortices are formed and shed in a complex and unsteady wake. As shown in Fig. 1 C and E, the eroded body comprises a conelike front with attached flow, a facet between separation ridges that is associated with quiescent flow, and a backside that has been scoured remarkably flat by the wake. The pointed nose and angular ridges are left protruding from the body, indicating relatively slow removal rates at these sites. Stagnation and separation are also known to be associated with low shear stress (14), suggesting that the flow's effectiveness in removing material is related to its shearing action.

We investigate this idea by using an arrangement in which the local erosion rate can be measured under conditions of known shear stress. A thin, flat bed of clay is spread evenly over a clear plate, which is then aligned with the flow. Photographs of the broad side of the plate show that the bed erodes more quickly at its upstream end, yielding a distinct interface that sweeps downstream while developing variations, as shown in Fig. 2A. The increasing spacing between successive interfaces indicates that the front accelerates, as quantified by measuring its mean position X versus time t for three trials (linear-scale plot in the inset of Fig. 2B). A logarithmic-scale plot reveals that, after an entry region of several millimeters, the front motion is consistent with uniform acceleration, $X \sim t^2$.

To arrive at a law relating erosion rate and shear stress, this motion must be reconciled with the shear stress dependence on the streamwise position. For high-speed flows, shear is associated with a boundary layer in which the velocity grows from zero at a surface and approaches the outer flow value of U at a characteristic distance δ (Fig. 2C). The Blasius solution describes the boundary-layer thickness along a plate (12), which grows with the streamwise coordinate as $\delta \sim x^{1/2}$, resulting in shear that decreases as $U/\delta \sim x^{-1/2}$. If the local erosion rate varies directly with shear stress, then $\dot{h} = -Cx^{-1/2}$ and thus $h(x,t) = h_0 - Cx^{-1/2}t$, where $h(x,t)$ is the local bed thickness, $h(x,0) = h_0$ is the initial thickness, and C is a constant. The interface is located where the bed has just eroded through, so that $h(X,t) = 0$ and $X = (C/h_0)^2 t^2$. Uniform acceleration thus results from the proportionality of erosion rate and shear stress, a law that is consistent with bulk measurements of other cohesive materials (15). Our direct determination of this

PHYSICS
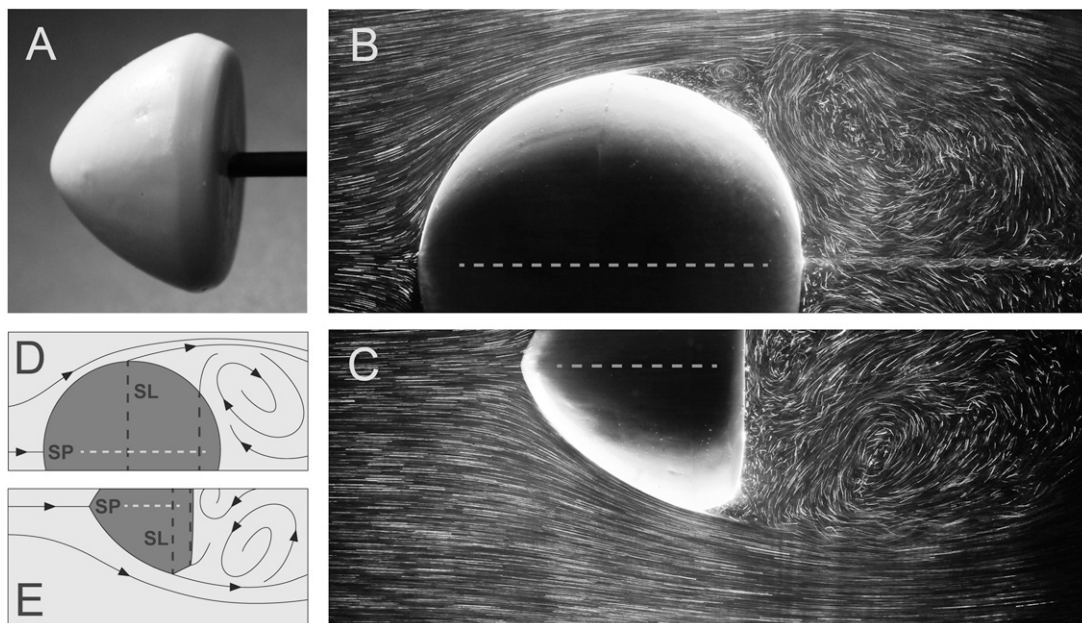
Fig. 1. Erosive sculpting of a clay sphere by flowing water. The flow speed is 46 cm/s and initial diameter 4.9 cm. (*A*) Removed after 70 min of erosion in a water tunnel, the body has a conelike nose, angular ridges, and flattened back. (*B* and *C*) Photographs of 10-ms exposure reveal streaklines at 10 and 70 min. The flow (left to right) conforms to the body before separating and forming a complex wake downstream. (*D* and *E*) Schematics show that the sharp features at the nose and ridges are associated with the flow stagnation point (SP) and separation lines (SL), respectively.

law's local validity is crucial for understanding cases in which the coevolving shape and flow strongly influence one another (12, 13).

Flow past a cylinder of clay provides a canonical, 2D setting in which the implications of the rate-stress erosion law can be

Fig. 2. Erosion of a clay bed reveals the dependence on shear stress. A 1-mm-thick layer of clay is spread over a clear plastic plate, which is aligned with the 61-cm/s flow. The bed first erodes away at its upstream end, resulting in an interface that sweeps downstream. (*A*) Interfaces extracted from photographs are displayed every 200 s and color-coded in time (flow from left to right). To avoid end effects in the cross-stream dimension, only the central 2.5-cm portion is analyzed. (*B*) Linear (inset) and logarithmic scale plots of the mean streamwise position of the front versus time for three trials. Relative variations in the interface position are typically less than 10%, and all trials are consistent with uniform acceleration (with slope of 2) after an entry region of several millimeters. (*C*) Qualitative schematic of flow past a plate. The local boundary layer thickness δ and outer flow speed U determine the shear, U/δ. For the experimental flow conditions, δ is predicted to be 0.1–1 mm.

investigated. For a body of initial diameter 3.6 cm immersed in a 61-cm/s flow, the time evolution of its cross-section is shown in Fig. 3*A*. The measured shrinkage rate can be compared with a prediction based on boundary-layer theory and the experimentally determined erosion law. Neglecting the details of shape, a body of typical length L has a boundary-layer thickness that scales as $\sqrt{L}$ and shear stress as $1/\sqrt{L}$. The product of stress and the exposed perimeter length gives the area reduction rate, $\dot{A} \sim -L/\sqrt{L} = -\sqrt{L} \sim -A^{1/4}$. This scaling analysis predicts that $A = A_0(1 - t/t_f)^{4/3}$, decreasing from an initial value of A_0 and vanishing at time t_f. As shown in Fig. 3*B* and its inset, this prediction (dashed red curves) accounts for the gradual slowing of mass loss measured in the experiment (black).

A striking and unexpected feature of the interfaces shown in Fig. 3*A* is the persistence of the quasi-triangular shape as the body erodes. Rescaling and shifting the interfaces so as to have the same area and same leading point (Fig. 3*C*) reveals that their upstream portions tend toward an angular shape, whereas the back slowly flattens. Thus, we discover that erosion proceeds self-similarly in time: After a transient morphing, the wedgelike front recedes while maintaining its shape.

Analysis of the flow around an ideal wedge of infinite extent gives insight into this emergent morphology. Here, we invoke the Falkner-Skan family of similarity solutions to the boundary-layer equations, which predict how shear stress varies along the surface (14, 16). Slender wedges have highest stress at their upstream end, whereas wide bodies have higher stress downstream. A right-angle wedge is unique in that its stress is identical at all points along the body, which would give rise to self-similar shrinking during erosion. The resemblance of the experimental shapes in Fig. 3 *A* and *C* to a right-angle wedge offers support to the idea of stress uniformity. This picture is further corroborated by measuring the erosion rate along the body. In the upper panel of Fig. 3*D*, we compare the erosion rate, measured as a function of arc length, for an early time (red) and later (blue) after the self-similar regime has set in. Whereas the early shape has spatially varying rate, the wedgelike body erodes more evenly from the nose to the separation corner (dashed vertical line).

Fig. 3. Evolution of an erodible cylinder. Clay is molded into a cylinder of diameter 3.6 cm, placed in the 61-cm/s flow, and photographed every minute from a view along its axis. (*A*) Extracted interfaces displayed every 5 min and color-coded in time, with flow from left to right. (*B*) The measured cross-sectional area (solid black curve) matches the theoretical prediction (dashed red). *Inset*: Logarithmic-scale plot of normalized area and time. (*C*) Equal-area rescaling of the interfaces reveals self-similar dynamics. The wedgelike front forms by about 45 min and then persists. (*D*) Erosion rate and computed shear stress along the body for early (red) and late (blue) times. *Upper*: The normal velocity of the interface is plotted against arc length, where 0 is the front, 0.5 the back of the body, and flow separation points are marked by the dashed vertical lines. *Lower*: Shear stress computed by simulating the flow around the experimentally extracted shapes.

To provide more direct evidence for stress uniformity, we use a computational method to analyze the flow around finite bodies. Our simulation determines local shear stress by combining a model of the outer flow with solutions to the boundary layer velocity profile. Importantly, the computed outer flow includes the effects of flow separation and a wake, as detailed in *Methods*. In Fig. 4*A*, we highlight key features of the simulated flow around the experimentally extracted body shape. The streamlines (solid lines) become more closely spaced as they deflect around the body and its wake (blank), indicating accelerating flow outside of the boundary layer (dark gray). Upstream of separation, the shear is related to this external velocity and to the local boundary-layer thickness, plotted as a function of arc length in Fig. 4*B*. Both velocity and thickness increase along the body, suggesting that their ratio U/δ is relatively constant. Indeed, as shown in the lower panel of Fig. 3*D*, the computed shear stress as a function of arc length for the eroded shape (blue) is flat in comparison with that of the initial shape (red). For both shapes, an apparent discrepancy occurs at the front, where the predicted stress is zero but the measured erosion rate is relatively high. Here, small-scale flow fluctuations may be responsible for rounding the nose of the body.

Our discovery of the uniform-stress morphology as an attracting state of erosion indicates the presence of a stabilizing effect in the flow–structure interaction. This feedback mechanism can be intuited by considering the effect of perturbations to an eroding surface. If some site on the boundary were to have higher stress than its neighbors, it would recede more quickly, which in general will shield the site from the flow and thus diminish its stress. Likewise, a site of low stress will be exposed as nearby locations erode, again causing conformity of stress. This argument does not seem restricted to particular flows or geometries. For example, when conditions are isotropic, as might be expected for Newton's wave-tossed pebbles, round shapes will likely prevail. The more general principle, however, appears to be a tendency not toward smoothness of shape but rather smoothness of stress.

Future studies might investigate whether sharp features, temporal self-similarity, and stress conformity appear in other scenarios, such as at low Reynolds number or for flows confined within erodible boundaries. Our findings would offer a powerful simplification in that steady-state morphology could be explained or

Fig. 4. Simulation of the flow around an eroded body. (*A*) For the experimentally extracted shape of Fig. 3 ($t = 100$ min), free-streamline and boundary-layer theories are used to compute the flow field. The streamlines (black) become compressed as they deflect around the body, indicating accelerating flow. A thin boundary layer (dark gray) develops in front and a stagnant wake (blank) sits downstream. (*B*) Computed boundary-layer thickness (dashed curve) and flow profiles, shown at two selected points. The flow speed matches the local outer flow value U at a distance δ. Both U and δ increase along the body, yielding similar slopes (darkened) of the flow profiles at the surface and thus nearly uniform shear.

predicted by seeking shapes that wear evenly. Finally, we were pleasantly surprised to find a possible natural analog for our studies, one that suggests these concepts apply more generally. In particular, so-called oriented meteors are thought to maintain a fixed posture as they descend through the atmosphere, experiencing intense aerodynamic heating that melts and ablates the surface (17). The meteorites that arrive on Earth bear a broad-angled nose that resembles the erosion sculpture of Fig. 1*A*. Further, the reported 100° opening angle for meteorites (18) is intriguingly similar to the 106° cone that 3D, axisymmetric Falkner-Skan theory predicts to have uniform stress (16). Although the underlying physical processes for erosion and ablation are different, it may be that both belong to a broader class of moving boundary problems in which surface evolution is dictated by shear stress.

Methods

Experiment. Soft clay is made from a 3:2 mixture by weight of water and bentonite nanoclay powder (Sigma-Aldrich). The flat bed is prepared by overfilling clay in the region between 1-mm-high spacers on a 15- × 15-cm Plexiglas plate and then scraping off the excess. The cylinder and sphere are molded on a lathe: Clay is first pasted onto a support rod, which is then spun while removing material by passing a taut wire along the surface. All preparations are eroded within the 15- × 15- × 43-cm (width × height × length) test section of a water tunnel (Engineering Laboratory Design, Inc.). Flow speed is continuously monitored with a laser Doppler velocimeter (TSI), with typical values between 40 and 70 cm/s maintained to within 1 cm/s for a given run. Water temperature is kept at 28 ± 1 °C. The water tunnel is constantly replenished with clean water to preserve imaging clarity. A digital camera captures time-lapsed images at a typical resolution of 40 pixels per millimeter, and flow is visualized using glass microspheres and a laser

sheet. MATLAB image analysis routines are used to extract and analyze the interfaces.

Simulation. Shear stress on the experimentally extracted shapes is computed by combining two classical methods. The outer flow is furnished by free-streamline theory, which then serves as the input to boundary-layer theory. Flow separation is modeled by free streamlines that extend from the body and enclose a stagnant wake, outside of which potential flow is assumed (19–21). The paths of the free streamlines as well as the complex potential—and thus the entire outer flow field—are determined by the Levi-Civita conformal mapping method. Boundary conditions include the following: Flow velocity is tangential at the body surface, pressure in the wake and along the free streamlines is equal to the far-field pressure, and the separation points are prescribed. Our simulation is not expected to apply near separation (22) but is robust provided that the high-curvature corner is confined to the wake. We therefore place the separation points upstream of the corner by 2% of the perimeter length and find consistent results if this value is doubled or halved. Given the computed outer flow, the boundary-layer velocity profile is approximated by the Pohlhausen method, which uses momentum integral balance to reduce the Prandtl equations to an ordinary differential equation for the boundary-layer thickness (14). Upstream of separation, shear stress is extracted from the near-body velocity profile. Past separation, the shear stress is zero due to the stagnant wake assumption, a simplification that is in qualitative accordance with the observed slow erosion on the backside.

1. Brewster D (1855) *Memoirs of the Life, Writings, and Discoveries of Sir Isaac Newton* (Harper, New York).
2. Huggett RJ (2011) *Fundamentals of Geomorphology* (Taylor & Francis, New York).
3. Yalin MS (1976) *Mechanics of Sediment Transport* (Pergamon, Oxford).
4. Melosh HJ (2011) *Planetary Surface Processes* (Cambridge Univ Press, Cambridge, UK).
5. Malin MC, Carr MH (1999) Groundwater formation of martian valleys. *Nature* 397 (6720):589–591.
6. Tomasko MG, et al. (2005) Rain, winds and haze during the Huygens probe's descent to Titan's surface. *Nature* 438(7069):765–778.
7. Huppert HE (1986) The intrusion of fluid mechanics into geology. *J Fluid Mech* 173: 557–594.
8. Rayleigh L (1944) Pebbles of regular shape and their production in experiment. *Nature* 154:169–171.
9. Schumm SA, Khan HR (1971) Experimental study of channel patterns. *Nature* 233 (5319):407–409.
10. Schorghofer N, Jensen B, Kudrolli A, Rothman DH (2004) Spontaneous channelization in permeable ground: Theory, experiment, and observation. *J Fluid Mech* 503: 357–374.
11. Zhang J, Libchaber A (2000) Periodic boundary motion in thermal turbulence. *Phys Rev Lett* 84(19):4361–4364.
12. Brivois O, Bonelli S, Borghi R (2007) Soil erosion in the boundary layer along a slope: A theoretical study. *Eur J Mech BFluids* 26(6):707–719.
13. Golay F, Lachouette D, Bonelli S, Seppecher P (2011) Numerical modeling of interfacial soil erosion with viscous incompressible flow. *Comput Methods Appl Mech Eng* 200:383–391.
14. Schlichting H (1968) *Boundary-Layer Theory* (McGraw-Hill, New York).
15. Grabowski RC, Droppo IG, Wharton G (2011) Erodibility of cohesive sediment: The importance of sediment properties. *Earth Sci Rev* 105(3–4):101–120.
16. Evans HL (1968) *Laminar Boundary-Layer Theory* (Addison-Wesley, Reading, MA).
17. Feldman S (1959) On the instability theory of the melted surface of an ablating body when entering the atmosphere. *J Fluid Mech* 6(1):131–155.
18. Kalashnik VN, et al. (1981) On the shape of bodies ablating in a supersonic gas stream. *Fluid Dyn* 16(1):11–14.
19. Hureau J, Brunon E, Legallais P (1996) Ideal free streamline flow over a curved obstacle. *J Comput Appl Math* 72(1):193–214.
20. Alben S, Shelley M, Zhang J (2002) Drag reduction through self-similar bending of a flexible body. *Nature* 420(6915):479–481.
21. Alben S, Shelley M, Zhang J (2004) How flexibility induces streamlining in a two-dimensional flow. *Phys Fluids* 16(5):1694–1713.
22. Sychev VV, Ruban AI, Sychev VV, Korolev GL (1998) *Asymptotic Theory of Separated Flows* (Cambridge Univ Press, Cambridge, UK).